

Hidden geometry and dynamics of complex networks: Spin reversal in nanoassemblies with pairwise and triangle-based interactions

Bosiljka Tadić^{1,2}, Neelima Gupte³

¹ *Department of Theoretical Physics, Jozef Stefan Institute, Ljubljana, Slovenia*

² *Complexity Science Hub Vienna, Josephstadtstrasse 39, Vienna, Austria and*

³ *Indian Institute of Technology Madras, Chennai, India*

(Dated:)

Recent studies of networks representing complex systems from the brain to social graphs have revealed their higher-order architecture, which can be described by aggregates of simplexes (triangles, tetrahedrons, and higher cliques). Current research aims at quantifying these hidden geometries by the algebraic topology methods and deep graph theory and understanding the dynamic processes on simplicial complexes. Here, we use the recently introduced model for geometrical self-assembly of cliques to grow nano-networks of triangles and study the field-driven spin reversal processes on them. With the antiferromagnetic interactions between the Ising spins attached to the nodes, this assembly ideally supports the geometric frustration, which is recognized as the origin of some new phenomena in condensed matter physics. In the dynamical model, a gradual switching from the pairwise to triangle-based interactions is controlled by a parameter. Thus, the spin frustration effects on each triangle give way to the mesoscopic ordering conditioned by a complex arrangement of triangles. We show how the balance between these interactions changes the shape of the hysteresis loop. Meanwhile, the fluctuations in the accompanying Barkhausen noise exhibit robust indicators of self-organized criticality, which is induced by the network geometry alone without any magnetic disorder.

I. INTRODUCTION

The influence of network structure on dynamics in many complex systems has been demonstrated in numerous studies with detailed analysis of empirical data and theoretical approaches [1–10]. Hence, the origin of structure of many complex networks can be sought in their evolutionary optimisations towards efficient functioning. Recently, numerous studies revealed that complex systems obey higher-order connectivity that can be described by simplexes of different sizes, see a recent overview in [11]. Beyond standard graph-theory methods [12], the aggregate simplicial complexes are suitably described by Q-analysis [13] based on the algebraic topology of graphs [14]. Some striking examples include human connectomes [15, 16] and (multi)-brain networks originating from experimental signals [17–19]. The higher-order interactions based on simplexes appear as constitutive characteristics of complex systems from biology [20], materials science [21–25] and physics [26, 27] to the large-scale social dynamics [28–31].

Current research of complex networks with hidden structures highlights three major directions. Specifically,

- exploring empirical data to discover the higher-order structures and the related dynamical patterns in them (Q-analysis, persistent homology, topological information data analysis) [11, 20, 32];
- theoretical investigations of different stochastic processes taking part on such structures to reveal the impact of higher-order structures and new phenomena that they may induce [31, 33, 34];
- modelling the assembly of networks with simplicial complexes to control the appearance of specific struc-

tural characteristics given altered function or dynamic processes that they can support. For example, pre-formatted groups, described as cliques (full graphs), are attached to a growing structure during the geometrically constrained process of self-assembly [1, 35, 36]. See the illustration in Fig. 1.

In materials science, the impact of the complex architecture of nano-materials to their functionality has been a subject of experimental investigations, which are often driven by the specific requirements for applications. A prominent example is the case of antiferromagnetic spintronics [37]. In this context, recent focus is on materials with complex architecture, like tetraborides [38] and artificial frustrated systems [39]. In such systems, the geometric constraints combined with the sign of the interactions prevent simultaneous minimisation of the global energy and each spin pair, leading to the spin frustration [40]. The geometric frustration effects have been shown to enable an unusual magnetic order and new dynamical phenomena in condensed matter physics [41–44] as well as in the Ising model applications [45, 46]. For example, one of the prominent features of spin frustration is the appearance of the fractional magnetisation plateaus in the hysteresis loop [38, 47, 48]. In [34], the nanonetworks of self-assembled mono-disperse cliques were studied. It was shown that, when endowed with antiferromagnetic bonds between pairs of spins on triangle faces, these assemblies provide ideal conditions for geometric frustration. The size of building simplexes directly affects the shape of the hysteresis loop, and the fractional magnetisation plateaus.

In this work, we study the spin-reversal dynamics on self-assembled nanonetworks with simplicial complexes in the presence of simplex-based interactions. More precisely, the network is grown by geometrical self-assembly of triangles as pre-formatted groups of nanoparticles, based on the self-

assembly model introduced in [1], and the Ising spin variable is attached to each node (nanoparticle). With antiferromagnetic interactions among pairs of neighbouring spins, the spin frustration effects are fully supported by the geometry of these simplexes [34]. Here, in addition to the pairwise interactions, we introduce a simplex-based interaction involving three spins on a triangle. Our motivation is to assess the impact of the higher-order interactions, which are naturally enabled by the structure of the assembly, by balancing them (via a parameter α) against the strong spin frustration effects promoted by the antiferromagnetic pairwise interactions on the same structure. We analyse their combined influence on the shape of the hysteresis loop and the multi-scale structure of the magnetisation fluctuations during the reversal process.

II. THE SELF-ASSEMBLY OF SIMPLEXES

The above mentioned Q-analysis reveals the geometric constituents of a simplicial complex in a given network. The generative models, on the other hand, offer a bottom-up approach to grow a structure with simplicial complexes controlled by pertinent parameters. In the prototype model introduced in [1], which we use here, the self-assembly of cliques is constrained by the geometric compatibility and chemical affinity factors (see also [36] for an extended model with defect cliques). More precisely, a simplex (clique) of the size $n \in [2, 10]$ is added by sharing one of its faces, i.e., sub-cliques of the size $n_q < n$, with an already existing clique in the growing structure. The faces of the order $q = 0, 1, 2, 3 \dots q_{\max} - 1$ indicate a single node, link, triangle, tetrahedron, and so on up to the largest sub-clique, where $q_{\max} = n - 1$ is the order of the added clique. The probability of a clique of the order q_{\max} to attach along its q -face is given by

$$P(q_{\max}, q; t) = \frac{c_q(t) e^{-v(q_{\max} - q)}}{\sum_{q=0}^{q_{\max}-1} c_q(t) e^{-v(q_{\max} - q)}}. \quad (1)$$

where v is the chemical affinity parameter, see Ref. [1] for a detailed description. The $c_q(t)$ is the number of geometrically compatible locations for docking a simplex of the order q , counted on the entire growing structure at the time t . The geometrical factor is weighted by the chemical affinity of the system towards the addition of $n_a = q_{\max} - q$ new nodes. Specifically, for a large $v < 0$, the system favours the addition of nodes. Thus the cliques preferably share a single node (see an example in Fig. 1 top panel). In the opposite limit, with increasing $v > 0$, the cliques progressively share their larger face; eventually, a single node can be added, leading to highly compact structures, as shown in [1, 36]. In the case when $v = 0$, the process is governed by the geometric compatibility factors alone. Consequently, each face can be shared with a finite probability, depending on its size and the actual network structure. See online demo on this link [49].

For this work, we grow an assembly of triangles under the strictly geometrical compatibility conditions ($q_{\max} = n - 1 = 2$, and $v = 0$). A close-up of the grown structure is depicted in the bottom panel of Fig. 1; it possesses 1000 nodes, 1737

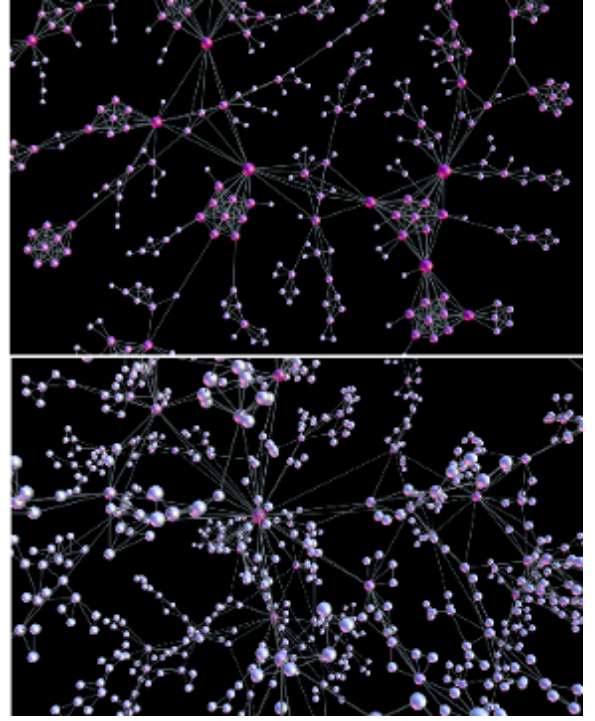


FIG. 1: Top: Zoom-in nanoparticle network self-assembled by preformatted groups of particles as cliques of different sizes $n \in [2, 10]$ for a negative chemical affinity v (significant repulsion between the cliques). Bottom: Self-assembled network of triangles for $v = 0$ (geometrically constraint self-assembly).

edges, and 738 triangles. As shown in [1, 36], these networks exhibit a broad distribution of the node's degree, assortative mixing, and a wide range of shortest-path distances between nodes (see Fig. 2). They also have the hyperbolic geometry (a negative curvature in the shortest-path metric space), precisely, they are 1-hyperbolic. The origin of the small hyperbolicity parameter in these networks is in the attachment of new clique via shared face with an existing clique. Thus, the distance between individual cliques, which are ideal hyperbolic structures ($\delta_{\text{clique}} = 0$), is minimal leading to $\delta_{\text{clique}} + 1$ -hyperbolic clique-complexes [50, 51]. We note that this attachment rule also prevents the appearance of holes in networks and that the order of a simplicial complex is equal to the order of the largest building simplex.

To study the magnetisation-reversal dynamics, here we adopt the network as shown in Fig. 1 bottom panel, and attach an Ising spin to each node (nanoparticle). The interactions among pairs of spins are enabled by the network links (adjacency matrix). Whereas, the triangle-based interactions are defined as *tri-spin interactions among spins situated on a given triangle*. In general, the triangle-adjacency matrix can be inferred by identifying all triangles, i.e., by performing the Q-analysis of the network [1, 36, 52]. In the present case, by growing the network in time steps t , we keep track of the nodes i_1, i_2, i_3 belonging to the added triangle. For example, in the first 11 steps, we can observe the following sequence of events (the variables in curly brackets are $\{t, N_t, \Sigma_t, n, n_a,$

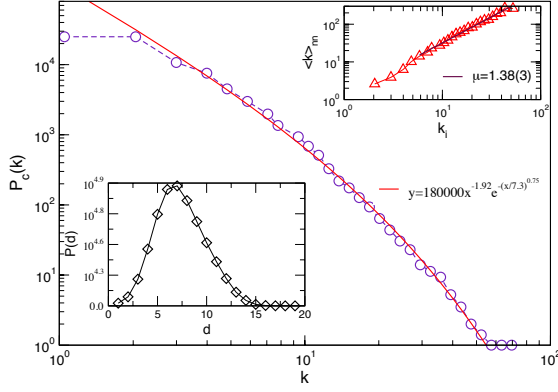


FIG. 2: For the network of self-assembled triangles: Sample averaged cumulative distribution $P_c(k)$ of the degree k (central panel) and the assortativity: the average degree of neighbour nodes plotted against the node's i degree (top inset), samples with 5000 nodes. Bottom inset: The distribution $P(d)$ of the shortest-path distances d , for the assembly with 1000 nodes.

i_1, i_2, i_3 , where n and n_a are defined above, and N_t and Σ_t stand for the number of nodes, and simplexes and faces, respectively.):

{1 3 7 3 2 1 2 3},
 {2 4 11 3 1 1 3 4}, {3 5 15 3 1 2 3 5},
 {4 6 19 3 1 1 3 6}, {5 7 23 3 1 3 4 7},
 {6 9 29 3 2 4 8 9}, {7 10 33 3 1 3 7 10},
 {8 11 37 3 1 8 9 11}, {9 12 41 3 1 3 10 12},
 {10 14 47 3 2 7 13 14}, {11 16 53 3 2 12 15 16}

III. SPIN REVERSAL DYNAMICS UNDER TRIANGLE-BASED INTERACTIONS

As mentioned in the Introduction, the antiferromagnetic spin-spin interactions in conjunction with a complex geometry of the assemblies provide ideal conditions for the spin frustration effects [34]. Here, we study the spin reversal dynamics driven by the external field h_{ext} on an assembly of triangles, cf. Fig. 1. Each pair of adjacent spins obeys antiferromagnetic interaction, whereas the higher-order interaction involves the spins based on the same triangle. The Hamiltonian is given by

$$\mathcal{H} = (\alpha - 1) \sum_{i,j} J_{ij} S_i S_j - \alpha \sum_{\langle i,j,k \rangle} K_{ijk} S_i S_j S_k - h_{ext} \sum_i S_i \quad (2)$$

where the Ising spins $S_i = \pm 1$ are associated with the network vertices; the summation in the first term is over all pairs of spins that have a link in the network's adjacency matrix, whereas the sum in the second term runs over the identified triangles, as described above. The spin-spin interaction $J_{ij} = -J$ is antiferromagnetic, whereas $K_{ijk} = K_3$ for the simplex-based interaction, where we consider both $K_3 > 0$ as well as $K_3 < 0$ cases. The parameter $\alpha \in [0, 1]$ is varied to provide a relative balance between the pairwise and higher-order interactions. We use the dimensionless units and set $J = 1$ and

$K_3 = \pm 1$. The magnetisation (in Bohr magnetons μ_B) is determined by the balance of the up and down oriented spins, $M = (N_+ - N_-)/N \in [-1, 1]$. Meanwhile, the external field h_{ext} (in the units $J\mu_B$) varies in the range $[-h_{max}, +h_{max}]$. The range relevant for the process is related to the maximum number of neighbours of the vertices.

The process is driven by slow ramping of the external field along an ascending/descending branch of the hysteresis loop. A zero-temperature dynamics is applied, as it is a widely accepted approach in the study of Barkhausen noise in disordered magnetic systems, see [53] and references therein. A small increase of the field can trigger an avalanche of spin reversal, during which each spin aligns along its local fields to minimise the energy. In the disordered ferromagnets, an avalanche of spin flips stops when the magnetic defects pin the domain wall of the expanding domain of reversed spins. In contrast, in the spin assemblies that we are studying here, there are no magnetic defects. Instead, the geometry of the network alone governs the progression of the spin reversal process (see also [34, 54]). Specifically, for the ascending branch, we start from a state with all spins down, and a large negative field $h_{ext} = -h_{max}$ is applied. $h_{max} \leq k_{max}$ correlates with the number of connections of the leading hub in the network. The field changes are *adiabatic*, which means that the field is kept fixed during the avalanche propagation. The field is increased in small steps Δ until it reaches the other limit $h_{ext} = +h_{max}$. Then the field is ramped by slow decreasing until it reaches $-h_{max}$ again, to complete the loop. Apart from the current value of the external field, the local field at the vertex i is given by the contribution of the actual states of the neighbouring spins according to the interactions in (2). In the present case, due to the fixed strength of the interactions, the local field changes in the integer values, which depend on the node's pairwise and triangle-based connectivity, modified by the parameter α . In analogy to modelling the charged domain-wall motion during the ferroelectric switching [55], the frustration effects within the zero-temperature dynamics are emulated by the probabilistic alignment between the spin and its local field with a probability $c < 1$. The results for the hysteresis loop are shown in Fig. 3 for several values of the parameter α , interpolating between the strictly pairwise antiferromagnetic interactions, for $\alpha = 0$, and strictly triangle-based interactions, for $\alpha = 1$.

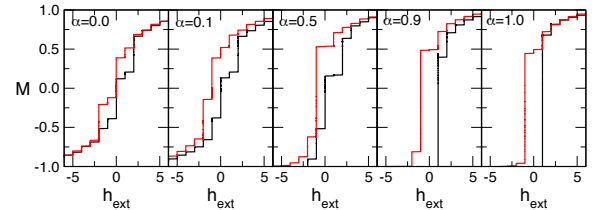


FIG. 3: Hysteresis loop in field-driven magnetisation reversal on the self-assembled network of triangles, see Fig. 1; different panels are for varied α from 0, corresponding to pure pairwise interaction to 1, entirely triangle-based interactions, see Eq. (2). Different colour indicates ascending and descending branches. The case with $K_3 > 0$ is shown.

As Fig. 3 shows, in the absence of the higher-order interactions, the hysteresis loop is symmetrical and, typically for the antiferromagnetic samples, splits into the positive and negative part. Moreover, the narrow tails at both high positive and high negative fields indicate the effects of a robust topological disorder, which permits only small avalanches of the reversed spins. The appearance of the higher-order interactions, however, induces a broadening and breaks the symmetry of the loop. In approaching the limiting case for $\alpha = 1$, the triangle-based interactions cause an entirely different shape of the hysteresis loop with a large rectangular part (resembling a ferromagnetic case). However, it also shows a disorder-conditioned tail, but on one side of the loop only. The implicated side depends on the sign of the K_3 , see also the inset in Fig. 4. Consequently, the increase of the magnetisation in time differs for the ascending and descending branch of the hysteresis whenever α is finite, as shown in the main panel of Fig. 4. For $\alpha = 1$, a similarity occurs between the magnetisation curves in different branches, but for the reversed sign of K_3 . More precisely, the ascending line for $K_3 > 0$ is a mirror reflection of a descending line for $K_3 < 0$, and also the ascending line for the case $K_3 < 0$ mirrors the descending line for $K_3 > 0$, cf. full red lines and the corresponding dashed pale lines in Fig. 4.

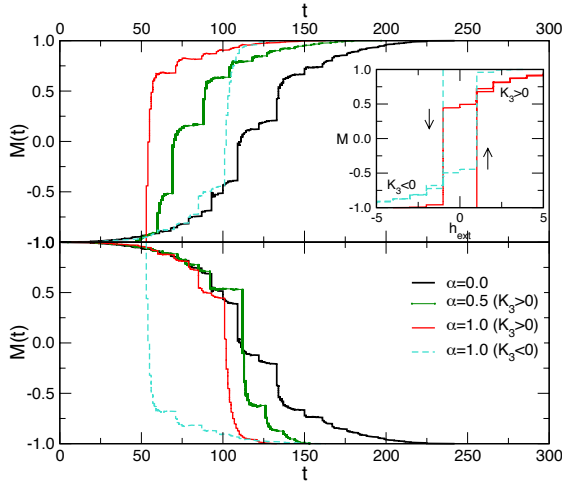


FIG. 4: Magnetisation versus time in the field-driven reversal processes on the self-assembled network of triangles, see Fig. 1; different panels are for varied α from 0, corresponding to pure pairwise interaction to 1, entirely triangle-based interactions, see Eq. (2). Ascending and descending branches are shown of separate panels for a better view. Inset: Hysteresis loop for $\alpha = 1$ (only triangle-based interactions) with $K_3 > 0$ and $K_3 < 0$.

The magnetisation fluctuations comprising the Barkhausen noise signals during the reversal processes for different α are shown in Fig. 5. The bursting events (avalanches) triggered by the changed of the external field have a characteristic triangular shape caused by the underlying geometry in the absence of disorder. With the increased α , we notice that the signal becomes shorter as well as its most massive avalanches occur much earlier, following the shape of the hysteresis loop in

Fig. 3. However, they all exhibit self-similarity with the long-range temporal correlations, as captured by the corresponding power-law behaviour of the power spectrum, $S(i) \sim i^{-\phi}$, cf. lower panel in Fig. 5. Furthermore, we find that these noise signals possess the multifractal features, similar to the Barkhausen noise in disordered ferromagnets [56]. More precisely, the fluctuation function $F_q(n)$ dependence on the segment length n of the signal exhibits a power-law behaviour with a spectrum of the exponents. In particular, dividing the signal in N_s segments and having defined the standard deviation $F(\mu, n) = \left\{ \frac{1}{n} \sum_{i=1}^n [Y((\mu-1)n+i) - y_\mu(i)]^2 \right\}^{1/2}$ around a local trend $y_\mu(i)$ in each segment $\mu = 1, 2 \dots N_s$, we have

$$F_q(n) = \left\{ \frac{1}{2N_s} \sum_{\mu=1}^{2N_s} [F^2(\mu, n)]^{q/2} \right\}^{1/q} \sim n^{H(q)} \quad (3)$$

Here, a generalised Hurst exponent H_q depends on the amplification factor q , as shown in Fig. 6. Intuitively, this means that the small fluctuations (amplified when $q < 0$) along the signal have different scaling properties than the large fluctuations ($q > 0$). In contrast, for the monofractal signals, $H_q = H_2$ for all q , where H_2 is the standard Hurst exponent. We note that a small variation in H_2 agree with small variations in the exponent of the power spectrum, hence the expected scaling relation $\phi = 2H_2 - 1$ is roughly satisfied (within the error bars).

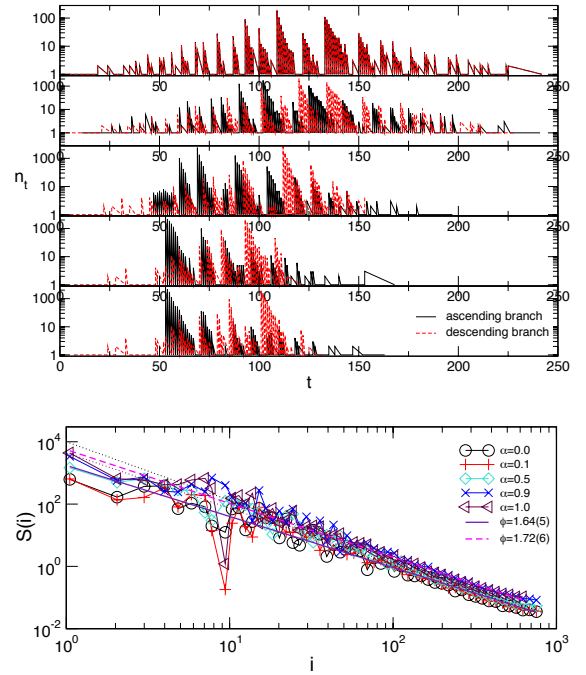


FIG. 5: Barkhausen noise signal n_t against time t in the field-driven reversal processes on the self-assembled network of triangles, see Fig. 1; five panels from the top are for different $\alpha \in [0, 1]$, from the pure pairwise interaction to entirely triangle-based interactions as in Fig. 3. Differences in the ascending and descending branches signal are indicated by colour. Bottom panel: Power spectrum of the signals (ascending branch) and their power-law fits, the maximum and minimum slopes are displayed.

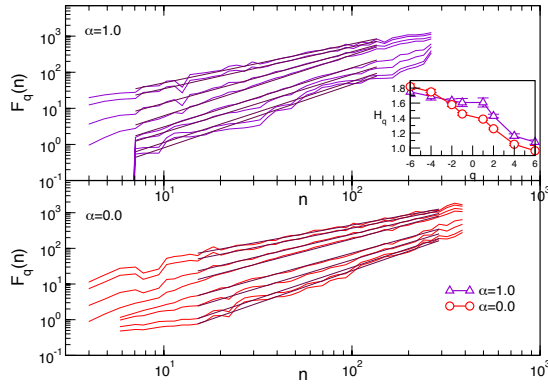


FIG. 6: Fluctuation function $F_q(n)$ vs. the segment length n for $q = 6, 4, 2, 1, -1, -2, -4, -6$ (top to bottom curve) for the ascending branch in the limiting cases $\alpha = 1.0$ and $\alpha = 0.0$. Inset: values of the generalised Hurst exponent H_q corresponding to the slope of the straight line indicated on each curve.

The critical behaviour at the hysteresis loop in disordered ferromagnets is often related to the occurrence of a critical disorder point or a critical line [53] in the parameters space. Even though signatures of the self-organised criticality are present. For a recent review of systems exhibiting self-organised criticality in [57] and references therein. As stated above, the avalanching process that we study here is governed by the geometry of the assembly without any magnetic disorder. Nevertheless, Fig. 5 and Fig. 6 demonstrate robust features of criticality in the magnetisation fluctuations. A detailed analysis of

scale invariance of the avalanches remains for separate work.

IV. CONCLUSIONS

We have briefly presented the subjects of current compelling research directions aiming to understand the role of the higher-order connectivity and interactions in the architecture and functional properties of complex systems. As a representative example, we have studied the nano-network grown by self-assembled simplexes (triangles), and the field-driven magnetisation reversal on them. With the antiferromagnetic interactions among the adjacent spin pairs and the triangle-based three-spin interactions, the underlying architecture enables the geometric frustration effects that have a pronounced impact on the hysteresis loop in these assemblies. By balancing between the pairwise and triangle-based interactions, the geometric frustration effects are gradually overridden by structural inhomogeneities due to the architecture of simplicial complexes. Moreover, the observed fluctuations of the magnetisation show a robust signature of self-organised criticality. The avalanching processes are conditioned solely by the geometry of the assembly without any magnetic disorder. These findings are in the line of research of complex nano-assembled materials with emerging functional properties.

Acknowledgments

Work supported by the Slovenian Research Agency under the Program P1-0044.

- [1] Šuvakov M., Andjelković M., Tadić B., Scientific Reports 8 (2018) 1987.
- [2] Dorogovtsev S. N., Goltsev A. V., Mendes J. F. F., Rev. Mod. Phys. 80 (2008) 1275.
- [3] Šuvakov M., Tadić B., Journal of Physics: Condensed Matter 22 (2010) 163201.
- [4] Krioukov D., Papadopoulos F., Kitsak M., Vahdat A., Boguñá M., Phys. Rev. E 82 (2010) 036106.
- [5] Živković J., Tadić B., Mathematics of Quantum and Nanotechnologies (Nanoscale Systems) 2 (2013) 30.
- [6] Andjelković M., Gupte N., Tadić B., Phys. Rev. E 91 (2015) 052817.
- [7] Castellano C., Pastor-Satorras R., Phys. Rev. X 7 (2017) 041024.
- [8] Dankulov M. M., Tadić B., Melnik R., Phys. Rev. E 100 (2019) 012309.
- [9] Millán A. P., Torres J. J., Bianconi G., Physical Review E 99 (2019) 022307.
- [10] Chutani M., Rao N., Nirmal Thyagu N., Gupte N., Chaos: An Interdisciplinary Journal of Nonlinear Science 30 (2020) 013109.
- [11] Maletić S., Zhao Y., Simplicial Complexes in Complex Systems: The Search for Alternatives (Harbin Institute of Technology, Harbin, P.R. of China) 2017.
- [12] Bollobás B., Modern Graph Theory (Springer, New York, inc.) 1998.
- [13] Beaumont J., Gatrell A., An Introduction to Q-Analysis (Geo Abstracts, Norwich-Printed by Edmund Nome Press, Norwich) 1982.
- [14] Jonson J., Simplicial Complexes of Graphs (Lecture Notes in Mathematics, Springer-Verlag, Berlin) 2008.
- [15] Tadić B., Andjelković M., Melnik R., Scientific Reports 9 (2019) 12060.
- [16] M. Andjelković, B. Tadić R. M., Scientific Reports 10 (2020) 17320.
- [17] Tadić B., Andjelković M., Boshkoska B. M., Levnajić Z., PLOS ONE 11 (2016) e0166787.
- [18] Tadić B., Andjelković M., Šuvakov M., Frontiers in Physics 6 (2018) 7.
- [19] Gupte N., Thyagu N. N., Chutani M., The simplicial characterisation of ts networks: Theory and applications in proc. of the 4th International Conference on Applications in Nonlinear Dynamics (ICAND 2016), edited by In V., Longhini P., Palacios A. (Springer International Publishing, Cham) 2017 pp. 289–296.
- [20] Baudot P., Tapia M., Bennequin D., Goillard J.-M., Entropy 21 (2019) 869.
- [21] Whitesides G. M., Grzybowski B., Science 295 (2002) 2418.
- [22] Boles M. A., Engel M., Talapin D. V., Chemical Reviews 116 (2016) 11220.

- [23] Wang Y., Wang Y., Breed D. R., Monaharan V. N., Feng L., Hollingsworth A., Weck M., Pine D., Nature 491 (2012) 51.
- [24] Fan X., Chung J. Y., Lim Y. X., Li Z., Loh X. J., ACS Applied Materials and Interfaces 8 (2016) 33351.
- [25] Kotani M. I. S., Science and Technology of Advanced Materials 17(1) (2016) 253.
- [26] Bianconi G., Rahmede C., Wu Z., Phys. Rev. E 92 (2015) 022815.
- [27] Tadić B., Andjelković M., Šuvakov M., Journal of Coupled Syst. Multiscale Dynamics 4 (2016) 30.
- [28] Andjelković M., Tadić B., Maletić S., Rajković M., Physica A: Statistical Mechanics and its Applications 436 (2015) 582.
- [29] Andjelković M., Tadić B., Mitrović Dankulov M., Rajković M., Melnik R., PLOS ONE 11 (2016) e0154655.
- [30] Tadić B., European Journal of Physics 40 (2019) 024002.
- [31] Wang D., Zhao Y., Leng H., Small M., Physics Letters A 384 (2020) 126895.
- [32] Petri G., Expert P., Turkheimer F., Carhart-Harris R., Nutt D., Hellyer P. J., Vaccarino F., Journal of The Royal Society Interface 11 (2014) 20140873.
- [33] Skardal P. S., Arenas A., Phys. Rev. Lett. 122 (2019) 248301.
- [34] Tadić B., Andjelković M., Šuvakov M., Rodgers G., Entropy 22 (2020) 336.
- [35] Bianconi G., Rahmede C., Scientific Reports 7 (2017) 41974.
- [36] Tadić B., Šuvakov M., Andjelković M., Rodgers G. J., Phys. Rev. E 102 (2020) 032307.
- [37] Jungwirth T., Marti X., Wadley P., Wunderlich J., Nature Nanotechnology 11 (2016) 231.
- [38] Brunt D., Balakrishnan G., Mayoh D., Lees M., Gorbunov D., Qureshi N., Petrenko O., Scientific Reports 8 (2018) 232.
- [39] Gilbert I., Nisoli C., Schiffer P., Physics Today 69 (2016) 54.
- [40] Diep H. T., Frustrated Spin Systems (World Scientific) 2005.
- [41] Mila F., Frustrated Spin Systems (E. Pavarini, E. Koch, and P. Coleman (eds.) Many-Body Physics: From Kondo to Hubbard Modeling and Simulation Vol. 5 Forschungszentrum Jülich, 2015.
- [42] Šl̂uētjes S. D., Urdahl H. H., Grepstad J. K., Folven E., AIP Advances 7 (2017) 056325.
- [43] Vanderstraeten L., Vanhecke B., Verstraete F., Phys. Rev. E 98 (2018) 042145.
- [44] Bang A. D., Hallsteinsen I., Olsen F. K., Šl̂uētjes S. D., Retterer S. T., Scholl A., Arenholz E., Folven E., Grepstad J. K., Applied Physics Letters 114 (2019) 192403.
- [45] Sheykhalı S., Darooneh A. H., Jafari G. R., Physica A: Statistical Mechanics and its Applications 548 (2020) 123882.
- [46] Krasnytska M., Bercheb B., Holovatcha Y., Kennad R., Nouse C., arxiv:2004.05134v1 (2020).
- [47] Dublenych Y. I., Phys. Rev. Lett. 109 (2012) 167202.
- [48] Lin W., Yang T., Wang Y., Qin M., Liu J.-M., Ren Z., Physics Letters A 378 (2014) 2565.
- [49] Šuvakov M., Andjelković M., Tadić B., Applet: Simplex Aggregated Growing Graph (<http://suki.ipb.rs/ggraph/>) 2017.
- [50] Bermudo S., Rodr̂guez J. M., Sigarreta J. M., Vilair J.-M., Discrete Mathematics 313 (2013) 1575.
- [51] Cohen N., Coudert D., Ducoffe G., Lancin A., Theoretical Computer Science 690 (2017) 114.
- [52] Freeman L. C., International Journal of Man-Machine Studies 12 (1980) 367.
- [53] Tadić B., Mijatović S., JaniĀĀević S., Spasojević D., Rodgers G. J., Scientific Reports 9 (2019) 6340.
- [54] Tadić B., Malarz K., Kułakowski K., Phys. Rev. Lett. 94 (2005) 137204.
- [55] Liu S., Grinberg I., Rappe A., Nature 534 (2016) 360.
- [56] Tadić B., Journal of Statistical Mechanics: Theory and Experiment 6 (2016) 063305.
- [57] Aschwanden M. (Editor), Self-Organized Criticality Systems (Open Academic Press Berlin Berlin Warsaw) 2013.